crystals

MDPI

*Article*

# Distinguishing the Focal-Conic Fan Texture of Smectic A from the Focal-Conic Fan Texture of Smectic B

**Natalia Osiecka-Drewniak [1,*], Zbigniew Galewski [2] and Ewa Juszyńska-Gałązka [1,3]**

[1] Institute of Nuclear Physics Polish Academy of Sciences, PL-31342 Cracow, Poland; ewa.juszynska-galazka@ifj.edu.pl
[2] Faculty of Chemistry, University of Wrocław, PL-50383 Wroclaw, Poland; zbigniew.galewski@chem.uni.wroc.pl
[3] Research Center for Thermal and Entropic Science, Graduate School of Science, Osaka University, Osaka 565-0871, Japan
* Correspondence: natalia.osiecka@ifj.edu.pl; Tel.: +48-12-662-84-81

**Abstract:** This publication presents methods of distinguishing the focal texture of the conical smectic phase A (SmA) and the crystalline smectic B phase (CrB). Most often, characteristic transition bars are observed in polarized light at the temperature point of the SmA–CrB phase transition. TOApy software transforms each image from a series of images recorded during POM observation to a function of light intensity versus temperature. Thermo-optical analysis is a powerful quantitative tool to notice this phase transition, but it has some limitations. The other applied method, the local binary pattern (LBP) algorithm, with high probability, detects differences between the textures of the conical focal fan of the SmA and CrB phases. The LBP algorithm is an efficient tool for texture classification.

**Keywords:** polarizing microscope; smectic A; smectic B; liquid crystals; local binary pattern algorithm



**Citation:** Osiecka-Drewniak, N.; Galewski, Z.; Juszyńska-Gałązka, E. Distinguishing the Focal-Conic Fan Texture of Smectic A from the Focal-Conic Fan Texture of Smectic B. *Crystals* **2023**, *13*, 1187. https://doi.org/10.3390/cryst13081187

Academic Editor: Pradip K. Bhowmik

Received: 30 June 2023
Revised: 25 July 2023
Accepted: 27 July 2023
Published: 30 July 2023



## 1. Introduction

Liquid crystals are considered a kind of soft matter that has anisotropic and viscoelastic properties. In liquid crystal phases, the molecules have some degree of order like those in a solid, but they can still flow and move around like those in a liquid. This results in a state of matter with intermediate properties between those of a liquid and a solid. Liquid crystals have different phases, including nematic, smectic, and cholesterol phases, each with unique characteristics based on the arrangement of the molecules. Many liquid crystal compounds have rich mesophase polymorphism [1–3]. The behavior of liquid crystals is sensitive to temperature, pressure, and electric field changes. These properties make them highly useful in various technological applications. Their most important application is the liquid crystal display (LCD) industry [4]. Liquid crystals are also a promising class of materials for other applications, such as biosensors [5], temperature indicators, paints, or opto-electronic devices [6]. Overall, liquid crystals have revolutionized the display industry and are an essential to modern electronic devices. The study of liquid crystal compounds exhibiting rich mesomorphism is important in basic science and various applications.

Several experimental methods can be used to detect the temperature range of mesophases. The simplest and most frequently used are the observations of textures with the help of a polarizing microscope (POM) as well as differential scanning calorimetry (DSC) [7–9]. An extremely powerful tool, more advanced, is X-ray diffraction (XRD) research. But unfortunately, this method most often fails with monotropic mesophases. The method called miscibility criterion also exists. The unknown phase of the new substance is mixed with a known phase of the reference sample. If no boundary is observed between them, it means that these phases are the same. In liquid crystal research, texture analysis with POM is the simplest, most essential, and most commonly used method. It requires a small sample mass and allows for monitoring the occurring changes in texture, which enables the identification of

mesophases. However, the assignment of the phase transition temperatures using only the POM technique is limited by the researcher's experience and the human eye's capabilities. For this reason, POM observations are equipped with a sophisticated analysis of recorded textures [10–12]. In addition, there are many similar textures with different mesophases as so-called paramorphic textures. An example of this problem is the focal conical fan texture of smectic phases A (SmA) and smectic phases B (SmB). In SmA, the molecules are arranged randomly in the layer, and the overall direction of the long molecular axes and the normal of the smectic layer are parallel. There are two types of B smectic phases: hexatic-B (HexB) and crystalline-B (CrB). The HexB phase's molecular ordering corresponds to the board-like structures' disordered hexagonal packing. The CrB phase is characterized by a long orientation order of molecules in smectic layers [13]. In the SmA phase, the appearance of focal conics is connected to the requirement of equidistance of fluid flexible layers. The focal surfaces in the packings of parallel equidistant curved layers transform into lines (confocal conics) to reduce the energy of singularities. In the SmB phase, there is an additional order within the layers. Typically, a focal conic fan texture of smectic B appears below the SmA with the same texture. Transition bars usually occur at the SmA–CrB phase transition. The lack of texture change during the SmA–HexB phase transition is a characteristic feature of the HexB phase [14]. The literature describes only a few substances with both HexB and CrB smectic phases [15,16].

The paper compares two methods used to distinguish the focal conic fan texture of the SmA phase from the focal conic fan texture of the CrB phase: TOA analysis and the local binary pattern (LBP) algorithm. One can find in literature publications where machine learning methods are used to classify liquid crystal textures [12,17–19]. Usually, chosen textures vary from each other.

## 2. Materials and Methods

For this study, three substances were chosen: 4-bromobenzylidene-4′-octyloxyaniline (8BBAA), 4-bromobenzylidene-4′-nonyloxyaniline (9BBAA), and 4-bromobenzylidene-4′-decyloxyaniline (10BBAA). Its polymorphism is well studied [17,20]. During cooling, the following phase transitions are observed: isotropic liquid phase (IL)–SmA, SmA–CrB, and CrB–crystalline (Cr) phase. All members of 4-bromobenzylidene-4′-alkyloxyaniline homologous series were synthesized in Prof. Galewski's group. The purity of the sample was 99%.

POM observations were performed using Leica DM2700P polarized light microscope. The temperature was stabilized by the Linkam T96-S temperature controller. The samples were sandwiched between two plates during cooling and heating runs, with a temperature rate of 10 °C/min.

Collected textures were converted into grayscale images and analyzed using TOApy and LBP algorithms [10,21]. The image resolution was equal to 2560 × 1920 pixels (px). Texture images were analyzed using a program written in the Python language (homemade by Natalia Osiecka-Drewniak, Cracow, Poland). An OpenCV implementation of the LBP algorithm was used [22]. The original images were converted into grayscale images. The accuracy of the LBP algorithm strongly depends on the number of images. Therefore, three chosen original images of each phase for each substance were cropped into 1200 images of SmA texture and 1200 images of CrB textures images. Textures of thermotropic liquid crystals exhibit self-similarity [23]. This feature allows one to manage the augmentation procedure by cropping [24]. Images resolution analyzed by the LBP algorithm was equal to 64 × 128 px. The data was divided into training and test datasets. The cross-validation method was used to estimate the model's accuracy and generalization capabilities. The process of cross-validation involves dividing all datasets into multiple subsets. The model is trained on subsets of the data and evaluated on the remaining data. This process was repeated ten times, with different subsets used for training and resting each iteration. One hundred images of each texture type of 8BBAA, 9BBAA, and 10BBAA were transferred into the test dataset.

## 3. Results and Discussion

The focal conic fan texture of SmA and CrB phases are presented in Figure 1. Distinguishing differences between textures of those mesophases by the human eyes is difficult. An experienced researcher will notice transition bars (see the middle column in Figure 1), a signature of the SmA–CrB phase transition. The transition bars appear and vanish quickly, which is characteristic of that phenomenon. Usually, the existence of transition bars is noticed in TOA thermograms (see Figure 2) as a collapse of light intensity between SmA and CrB phases. That dependence has been noticed in the case of 8BBAA and 10BBAA, but 9BBAA does not show it. Moreover, it is often noticed that the light intensity recorded for the focal conic texture of SmA has higher values than the light intensity noticed for the focal conic texture of the CrB phase [25]. Only 8BBAA compound follows that behavior. For 10BBAA, some texture of the SmA phase occurs higher light intensity than textures of the CrB phase and others lower. The light intensity of the focal conic fan texture of the SmA phase of 9BBAA does not differ from the focal conic fan texture of the CrB phase of 9BBAA. One can find in literature TOA thermograms where the light intensity in the frame of the same phase changes more rapidly than the light intensity shift observed between SmA and CrB phase transitions for the 8BBAA, 9BBAA, and 10BBAA compounds [26–28].

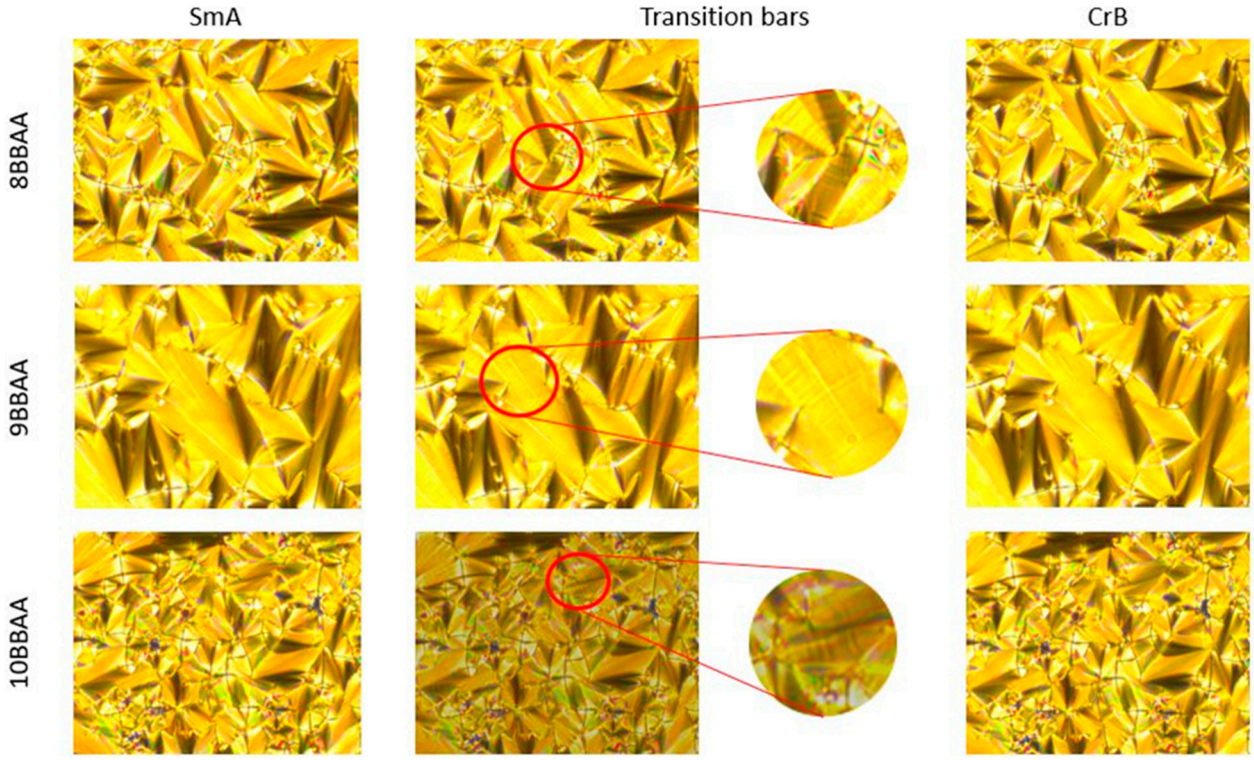


**Figure 1.** The focal conic fan texture of SmA and CrB phases and transitions bars separating both mesophases for 8BBAA, 9BBAA, and 10BBAA.

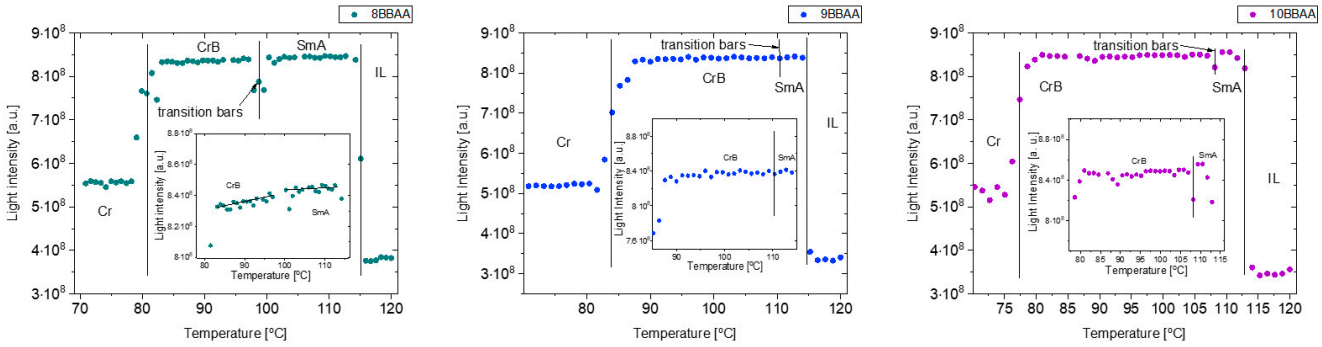


**Figure 2.** TOA thermogram for 8BBAA, 9BBAA, and 10BBAA compounds. Inserted figures show the enlarged region for the light intensity in CrB and SmA phases. The straight lines mark phase transition temperatures obtained from TOApy analysis of POM measurements.

The LBP method is a significant breakthrough in texture analysis. It is widely used for texture analysis and classification in computer vision and image classification. The basic idea behind the LBP algorithm is to encode an image's local structure or texture information by comparing the intensity values of a central pixel with its neighboring pixels. The scheme of the LBP algorithm is presented in Figure 3. At first, each pixel $g_c$ in the image is compared with a chosen number of neighboring pixel points ($P$) in a chosen distance, a radius R, from that pixel $g_c$ (see Figure 3a). The user chooses the $R$ and $P$ values. Next, the values of neighboring pixels $g_i$ are binarized (can take two possible values 0 or 1), due to the value of the central pixel $g_c$ following with Equation (1) (Figure 3b):

$$s(g_i) = \begin{cases} 1, & g_i \geq g_c \\ 0, & g_i < g_c \end{cases} \quad (1)$$

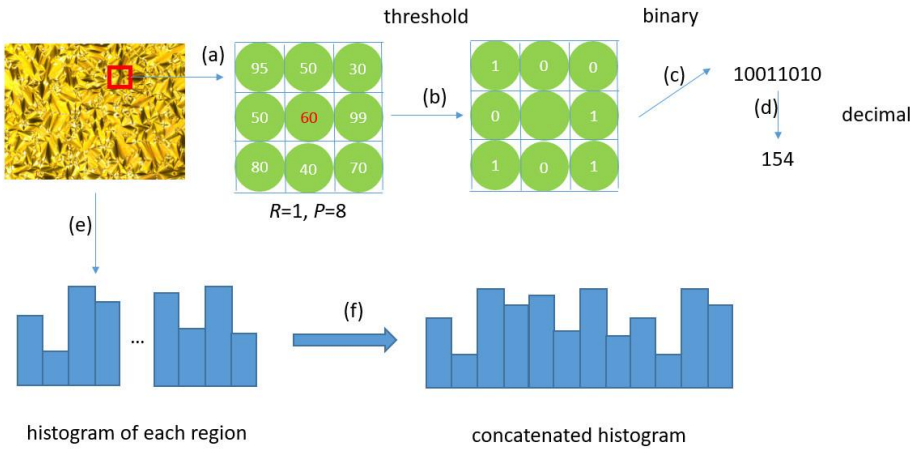


**Figure 3.** Schedule of LBP histogram.

Then, based on the binary values, the decimal value is obtained (Figure 3c,d), usually clockwise. This procedure can be described by the following Equation (2):

$$LBP_{P,R} = \int_{i=1}^{P} s(g_c - g_i)2^i \quad (2)$$

where $s$ is defined by Equation (1). After the LBP procedure of each pixel is calculated, a histogram to represent the texture image is built (Figure 3e,f) [29,30]. Support vector machines (SVM) were employed to develop the classification performance of LBP histograms. The SVM algorithm is designed to find an optimal hyperplane that best separates the data points belonging to different classes in the feature space. The hyperplane is chosen in

such a way that it maximizes the margin, which is the distance between the hyperplane and the nearest data points from each class. These nearest data points are called support vectors [31]. A comparison of the original image and the image after the LBP modification is presented in Figure 4.

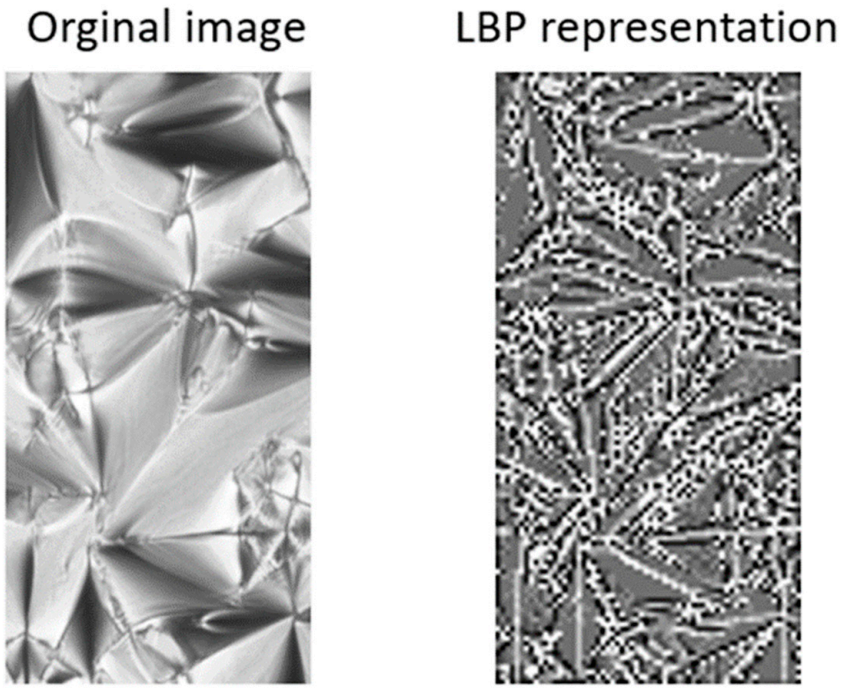


**Figure 4.** Comparison of original image (**left** image) and its LP representation (**right** image).

Distinguishing the texture of liquid crystals from each other is a classification issue. The LBP algorithm learns how to recognize each texture of a chosen phase from the training data. Evaluation of the LBP model is examined using the training data. Several metrics provide essential information about the model performance: accuracy, precision, and recall [32]. The description of those metrics consists of several terms: true positive (*TP*), true negative (*TN*), false positive (*FP*), and false negative (*FN*). TP are the number of instances correctly predicted as positive by the model. *TN* are the cases where the model correctly identifies negative samples as negative. *FP* are the instances where the model predicts positive when the actual label is negative. *FN* are the cases where the model predicts a negative when the actual label is positive. Figure 5 briefly presents those terms as a confusion matrix. The confusion matrix shows the evaluation of the classification model on the test data set. The objects (i.e., images) are assigned to various classes, and this information is compared to the original object labels. Accuracy is a ratio of correctly predicted observations to all elements in the data set. It is a commonly used evaluation metric in machine learning tasks. Accuracy is easy to understand and has an intuitive interpretation, while it measures the percentage of correct predictions made by a model out of the total predictions. This metric works well when the dataset has a roughly equal number of samples for each class. It is described by Equation (3):

$$accuracy = \frac{(TP + TN)}{(TP + TN + FP + FN)} \quad (3)$$

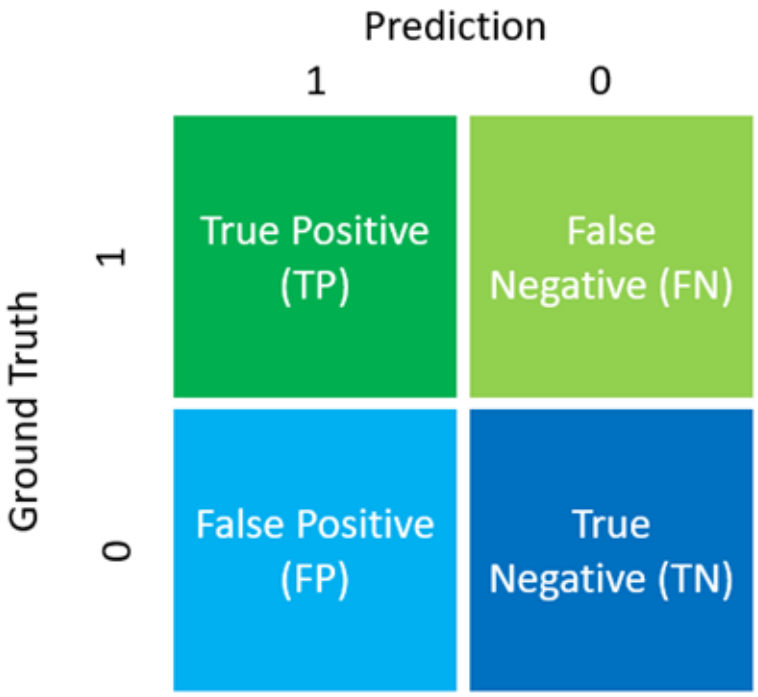


**Figure 5.** Confusion matrix for binary classification, where 0 and 1 are two different classes.

However, accuracy treats all errors equally, which may not align with the practical importance of certain misclassification. It does not distinguish between *FP* and *FN*. For this reason, it is essential to consider other evaluation metrics like precision and recall. Precision shows how well an algorithm can identify the *TP* from all that is predicted as positive:

$$precision = \frac{TP}{(TP + FP)} \tag{4}$$

Recall is ascribed as a ratio of correctly predicted positive observations to all observations in a given class:

$$recall = \frac{TP}{(TP + FN)} \tag{5}$$

The results of classification accuracy to SmA or CrB focal conic fan textures of 8BBAA, 9BBAA, and 10BBAA (considered together) using different LBP features are presented in Table 1. The maximum accuracy (0.85) was obtained for the following LBP parameters ($R$ = 4, $P$ = 28), ($R$ = 4, $P$ = 30), ($R$ = 4, $P$ = 32). The highest precision score (0.89) for the SmA phase was obtained for $R$ = 4 and $P$ = 30, while for CrB (0.84), LBP parameters were equal to $R$ = 4 and $P$ = 32. This information suggests that CrB textures occur in more false positive classifications than SmA textures. The maximum recall for SmA textures was obtained for the following LBP parameters $R$ = 4, $P$ = 32, while for CrB textures $R$ = 4, $P$ = 30. This observation indicates that SmA textures occur in more false negative classifications than CrB textures.

The LBP algorithm was also performed on each dataset textures of 8BBAA, 9BBAA and 10BBAA separately (see Tables 2–4). The highest accuracy score (0.94) was performed for 9BBAA, where LBP parameters were equal to $R$ = 4, $P$ = 28. *Precision* and *recall* (for $R$ = 4 and $P$ = 28) obtained similar values. Also, high accuracy score was noticed for 8BBAA textures (0.93) for LBP parameters $R$ = 3 and $P$ = 24. For those parameters, there is almost no difference between *precision* and *recall* values. The lowest accuracy scores were obtained for 10BBAA. The LBP methods give the best results (*accuracy* = 0.86) for $R$ = 3 and $P$ = 24. The LBP algorithm for $R$ = 3 and $P$ = 24 in the case of 10BBAA notices a higher precision value for SmA textures, while recall values are higher for CrB textures. This information

suggests that CrB textures result in more false positive classifications than SmA textures, while SmA textures show more false negative classifications than CrB textures.

**Table 1.** *Accuracy*, *precision*, and *recall* of focal conic fan texture classifications to SmA or CrB phases of 8BBAA, 9BBAA, and 10BBAA using the LBP model with selected radius and points values. The uncertainty of those parameters is equal ± 0.01.

| Radius | Points | *Accuracy* | *Precision* | | *Recall* | |
|---|---|---|---|---|---|---|
| | | | **SmA** | **CrB** | **SmA** | **CrB** |
| 1 | 4 | 0.66 | 0.74 | 0.60 | 0.55 | 0.79 |
| 1 | 6 | 0.76 | 0.81 | 0.71 | 0.72 | 0.81 |
| 1 | 8 | 0.80 | 0.80 | 0.87 | 0.75 | 0.75 |
| 2 | 8 | 0.81 | 0.81 | 0.86 | 0.77 | 0.78 |
| 2 | 10 | 0.81 | 0.81 | 0.84 | 0.77 | 0.79 |
| 2 | 12 | 0.79 | 0.79 | 0.82 | 0.76 | 0.78 |
| 2 | 14 | 0.83 | 0.83 | 0.86 | 0.80 | 0.82 |
| 2 | 16 | 0.83 | 0.83 | 0.88 | 0.78 | 0.79 |
| 3 | 24 | 0.83 | 0.83 | 0.86 | 0.80 | 0.81 |
| 3 | 20 | 0.84 | 0.84 | 0.87 | 0.80 | 0.82 |
| 3 | 16 | 0.83 | 0.83 | 0.86 | 0.81 | 0.83 |
| 3 | 12 | 0.84 | 0.84 | 0.88 | 0.81 | 0.82 |
| 4 | 26 | 0.84 | 0.84 | 0.88 | 0.81 | 0.82 |
| 4 | 28 | 0.85 | 0.85 | 0.88 | 0.81 | 0.83 |
| 4 | 30 | 0.85 | 0.85 | 0.89 | 0.82 | 0.83 |
| 4 | 32 | 0.85 | 0.85 | 0.87 | 0.84 | 0.85 |

**Table 2.** *Accuracy*, *precision*, *recall*, and score of focal conic fan texture classifications to SmA or CrB phases of 8BBAA using the LBP model with selected radius and points values. The uncertainty of those parameters is equal ± 0.01.

| Radius | Points | *Accuracy* | *Precision* | | *Recall* | |
|---|---|---|---|---|---|---|
| | | | **SmA** | **CrB** | **SmA** | **CrB** |
| 1 | 4 | 0.81 | 0.79 | 0.83 | 0.85 | 0.77 |
| 1 | 6 | 0.86 | 0.90 | 0.82 | 0.81 | 0.91 |
| 1 | 8 | 0.81 | 0.84 | 0.78 | 0.77 | 0.85 |
| 2 | 8 | 0.87 | 0.88 | 0.86 | 0.86 | 0.88 |
| 2 | 10 | 0.85 | 0.86 | 0.83 | 0.83 | 0.86 |
| 2 | 12 | 0.84 | 0.83 | 0.84 | 0.85 | 0.82 |
| 2 | 14 | 0.86 | 0.84 | 0.88 | 0.89 | 0.82 |
| 2 | 16 | 0.87 | 0.88 | 0.86 | 0.86 | 0.87 |
| 3 | 24 | 0.93 | 0.93 | 0.92 | 0.93 | 0.92 |
| 3 | 20 | 0.90 | 0.92 | 0.88 | 0.88 | 0.92 |
| 3 | 16 | 0.91 | 0.92 | 0.89 | 0.89 | 0.92 |
| 3 | 12 | 0.84 | 0.91 | 0.79 | 0.76 | 0.92 |
| 4 | 26 | 0.91 | 0.92 | 0.91 | 0.91 | 0.92 |
| 4 | 28 | 0.89 | 0.91 | 0.86 | 0.86 | 0.92 |
| 4 | 30 | 0.90 | 0.94 | 0.87 | 0.86 | 0.94 |
| 4 | 32 | 0.89 | 0.92 | 0.86 | 0.85 | 0.92 |

**Table 3.** *Accuracy*, *precision*, *recall*, and score of focal conic fan texture classification to SmA or CrB phases of 9BBAA using the LBP model with selected radius and points values. The uncertainty of those parameters is equal ± 0.01.

| Radius | Points | *Accuracy* | *Precision* | | *Recall* | |
|---|---|---|---|---|---|---|
| | | | **SmA** | **CrB** | **SmA** | **CrB** |
| 1 | 4 | 0.72 | 0.72 | 0.73 | 0.75 | 0.70 |
| 1 | 6 | 0.76 | 0.77 | 0.75 | 0.75 | 0.77 |
| 1 | 8 | 0.82 | 0.84 | 0.81 | 0.8 | 0.85 |
| 2 | 8 | 0.82 | 0.82 | 0.83 | 0.84 | 0.81 |
| 2 | 10 | 0.85 | 0.85 | 0.86 | 0.87 | 0.84 |
| 2 | 12 | 0.85 | 0.84 | 0.85 | 0.86 | 0.83 |
| 2 | 14 | 0.80 | 0.83 | 0.78 | 0.77 | 0.84 |
| 2 | 16 | 0.82 | 0.86 | 0.79 | 0.77 | 0.87 |
| 3 | 24 | 0.90 | 0.87 | 0.93 | 0.93 | 0.86 |
| 3 | 20 | 0.88 | 0.87 | 0.89 | 0.89 | 0.86 |
| 3 | 16 | 0.90 | 0.89 | 0.91 | 0.92 | 0.88 |
| 3 | 12 | 0.86 | 0.86 | 0.86 | 0.87 | 0.86 |
| 4 | 26 | 0.92 | 0.92 | 0.92 | 0.92 | 0.92 |
| 4 | 28 | 0.94 | 0.94 | 0.95 | 0.95 | 0.93 |
| 4 | 30 | 0.91 | 0.92 | 0.91 | 0.91 | 0.92 |
| 4 | 32 | 0.93 | 0.93 | 0.93 | 0.93 | 0.92 |

**Table 4.** *Accuracy*, *precision*, *recall*, and score of focal conic fan texture classification to SmA or CrB phases of 10BBAA using LBP model with selected radius and points values. The uncertainty of those parameters is equal ± 0.01.

| Radius | Points | *Accuracy* | *Precision* | | *Recall* | |
|---|---|---|---|---|---|---|
| | | | **SmA** | **CrB** | **SmA** | **SmB** |
| 1 | 4 | 0.68 | 0.76 | 0.63 | 0.53 | 0.83 |
| 1 | 6 | 0.84 | 0.93 | 0.78 | 0.75 | 0.94 |
| 1 | 8 | 0.76 | 0.85 | 0.70 | 0.64 | 0.88 |
| 2 | 8 | 0.80 | 0.82 | 0.79 | 0.79 | 0.82 |
| 2 | 10 | 0.78 | 0.81 | 0.76 | 0.75 | 0.81 |
| 2 | 12 | 0.78 | 0.76 | 0.79 | 0.81 | 0.74 |
| 2 | 14 | 0.82 | 0.80 | 0.84 | 0.86 | 0.78 |
| 2 | 16 | 0.80 | 0.80 | 0.80 | 0.81 | 0.80 |
| 3 | 24 | 0.86 | 0.89 | 0.84 | 0.84 | 0.89 |
| 3 | 20 | 0.85 | 0.85 | 0.85 | 0.85 | 0.84 |
| 3 | 16 | 0.82 | 0.83 | 0.81 | 0.81 | 0.83 |
| 3 | 12 | 0.79 | 0.82 | 0.77 | 0.76 | 0.82 |
| 4 | 26 | 0.84 | 0.88 | 0.81 | 0.80 | 0.89 |
| 4 | 28 | 0.83 | 0.87 | 0.80 | 0.80 | 0.87 |
| 4 | 30 | 0.82 | 0.85 | 0.79 | 0.78 | 0.86 |
| 4 | 32 | 0.79 | 0.83 | 0.76 | 0.75 | 0.84 |

## 4. Conclusions

The molecular arrangement in the SmA phase and CrB phase vary from each other in the smectic layers. The focal conic fan texture of those phases exhibits high similarity. TOA analysis and LBP algorithms are powerful methods that allow distinguishing the focal fan texture of SmA from CrB phases. However, the results of TOA analysis are subjective and depend on the researcher's experience. The results of the LBP algorithm are quantitative and qualitative. LBP techniques' accuracy in recognizing focal conic fan texture of the SmA phase and CrB phase for several substances is around 85% (for R = 4 and P = {28, 30, 32}). The accuracy prediction increases when textures of each phase are studied separately for each substance. The chosen values of the LBP algorithm (R and P) influence the classification accuracy. The highest texture classification accuracy for the

SmA or CrB phases for 8BBAA and 10BBAA was observed for R = 3 and P = 24. In the case of 9BBAA, the best LBP parameters were R = 4 and P = 28. For low R values, the accuracy of texture classification was also low. Focal conic texture also occurs for the SmC phase and is a signature of the appearance of the ferroelectric nematics [33]. The LBP algorithm could be applied to distinguish various focal conic phases.

**Author Contributions:** Conceptualization, N.O.-D.; software, N.O.-D.; investigation, N.O.-D.; resources, Z.G.; writing—original draft preparation, N.O.-D.; writing—review and editing, N.O.-D., Z.G. and E.J.-G. All authors have read and agreed to the published version of the manuscript.

**Funding:** This research received no external funding.

**Data Availability Statement:** The data presented in this study are available on request from the corresponding author.

**Conflicts of Interest:** The authors declare no conflict of interest.

## References

1. Lavrentovich, O.D. Transport of particles in liquid crystals. *Soft Matter* **2014**, *10*, 1264. [CrossRef] [PubMed]
2. de Gennes, P.G. Soft matter. *Science* **1992**, *256*, 495–497. [CrossRef]
3. Piwowarczyk, M.; Osiecka-Drewniak, N.; Gałązka, M.; Galewski, Z. Synthesis, mesogenic and photoisomerization studies of (E)-4-[(4-pentyloxyphenyl)diazenyl]phenyl alkanoates. *Phase Trans.* **2019**, *92*, 1066–1076. [CrossRef]
4. Cristaldi, J.R.D.; Pennisi, S.; Pulvirenti, P. *Liquid Crystal Display Drivers: Techniques and Circuits*; Springer: Berlin/Heidelberg, Germany, 2009.
5. Wang, Z.; Xu, T.; Noel, A.; Chen, Y.C.; Liu, T. Applications of liquid crystals in biosensing. *Soft Matter* **2021**, *17*, 4675. [CrossRef] [PubMed]
6. Lagerwall, J.P.F.; Scalia, G. A new era for liquid crystal research: Applications of liquid crystals in soft matter nano-, bio- and microtechnology. *Cur. App. Phys.* **2012**, *12*, 1387–1412. [CrossRef]
7. Pietrzyk, S.; Yevchenko, T.; Dardas, D.; Brańka, A.C. Phase transitons and physical properties by a color texture analysis: Results for liquid crystals. *J. Mol. Liq.* **2022**, *362*, 119699. [CrossRef]
8. Jasiurkowska-Delaporte, M.; Juszyńska, E.; Kolek, L.; Krawczyk, J.; Massalska-Arodź, M.; Osiecka, N.; Rozwadowski, T. Signatures of glass transition in partially ordered phases. *Liq. Cryst.* **2013**, *40*, 1436–1442. [CrossRef]
9. Poryvai, A.; Bubnov, A.; Pociecha, D.; Svoboda, J.; Kohout, M. The effect of the length of terminal n-alkyl carboxylate chain on self-assembling and photosensitive properties of chiral lactic acid derivatives. *J. Mol. Liq.* **2019**, *275*, 829–838. [CrossRef]
10. Osiecka, N.; Galewski, Z.; Massalska-Arodz, M. TOApy program for the thermooptical analysis of phase transitions. *Termochi. Acta* **2017**, *655*, 106–111. [CrossRef]
11. Orlikowska, H.; Sobolewska, A.; Miniewicz, A.; Bartkiewicz, S. Application of the novel dynamic thermos-optical analysis for identification of the sequence of mesophases in thermotropic liquid crystal. *Liq. Cryst.* **2017**, *44*, 1157–1164. [CrossRef]
12. Sigaki, H.Y.D.; de Souza, R.F.; de Souza, R.T.; Zola, R.S.; Ribeiro, H.V. Estimating physical properties from liquid crystal textures via machine learning and complexity-entropy methods. *Phys. Rev. E* **2019**, *99*, 013311. [CrossRef]
13. Repasky, P.J.; Agra-Kooijman, D.M.; Kumar, S.; Hartley, C.S. Smectic-A and hexatic-B liquid crystal phases of sandic alkyl-substituted dibenzo[fg,op]naphthacenes. *J. Phys. Chem. B* **2016**, *120*, 2829–2837. [CrossRef] [PubMed]
14. Goodby, J.W.; Pindak, R. Characterization of the hexatic B and crystal B phases by optical microscopy. *Mol. Cryst. Liq. Cryst.* **1981**, *75*, 233–247. [CrossRef]
15. Albertini, G.; Fanelli, E.; Melone, S.; Rustichelli, F.; Torquati, G. Evidence by X-ray diffraction for hexatic B and crystal B structures in a pure compound. *Solid State Comm.* **1984**, *49*, 1143–1146. [CrossRef]
16. Pyżuk, W.; Krówczynski, A.; Górecka, E. Novel series of enaminoketone liquid crystals having hexatic smectic B phase. *Mol. Cryst. Liq. Cryst.* **1993**, *237*, 75–84. [CrossRef]
17. Prasa, A.A.B.; Zola, R.A.; Perc, M.; Roberto, H.V. Determining liquid crystals properties with ordinal networks and machine learning. *Chaos Solitons Fractals* **2022**, *154*, 111607.
18. Sigaki, H.Y.D.; Lenzi, E.K.; Zola, R.S.; Perc, M.; Roberto, H.V. Learning physical properties of liquid crystals with deep convolutional neural networks. *Scient. Rep.* **2020**, *10*, 7664. [CrossRef]
19. Dierking, I.; Dominguez, J.; Harbon, J.; Heston, J. Deep learning techniques for the localization and classification of liquid crystals phase transitions. *Front. Soft. Matter* **2023**, *3*, 1114551. [CrossRef]
20. Osiecka, N.; Budziak, A.; Galewski, Z.; Massalska-Arodź, M. X-ray studies of the smectic B phase of the 4-bromobenzylidene-4'-alkoxyanilines. *Phase Trans.* **2012**, *85*, 314–321. [CrossRef]
21. Ojala, T.; Pietikainen, M.; Maenpaa, T. Multiresolution gray-scale and rotation invariant texture classification with local binary patterns. *IEEE Trans. Pattern Anal. Mach. Intell.* **2002**, *24*, 971–987. [CrossRef]
22. Bradski, G. The OpenCV Library. *J. Soft. Tools* **2000**, *120*, 122–125.

23. Massalska-Arodź, M. Scaling in 2-D distribution of topological defects in a liquid crystal. *Acta Phys. Pol. A* **1998**, *94*, 41–47. [CrossRef]
24. Shorten, C.; Khoshgoftaar, T.M. A survey on image data augmentation for deep learning. *J. Big Data* **2019**, *6*, 60. [CrossRef]
25. Galewski, Z.; Coles, H.J. Liquid crystalline properties and phase situations in 4-chlorobenzylidene-4′-alkylanilines. *J. Mol. Liq.* **1999**, *79*, 77–87. [CrossRef]
26. Osiecka, N.; Juszyńska-Gałązka, E.; Galewski, Z.; Jaworska-Golab, T.; Deptuch, A.; Massalska-Arodź, M. Insight into polymorphism of the ethosuximide (ETX). *J. Therm. Anal. Cal.* **2018**, *133*, 961–967. [CrossRef]
27. Chachaj-Brekiesz, A.; Gorska, N.; Osiecka, N.; Dynarowicz-Latka, P. Mesophases of non-convetional liquid crystalline molecules. *J. Therm. Anal. Cal.* **2016**, *126*, 689–697. [CrossRef]
28. Drzewicz, A.; Juszyńska-Gałązka, E.; Deptuch, A.; Kula, P. Effect of alkyl chain length on the phase situation of glass-forming liquid crystals. *Crystals* **2022**, *12*, 1401. [CrossRef]
29. Zhou, H.; Wang, R.; Wang, C. A novel extended local-binary-pattern operator for texture analysis. *Inform. Sci.* **2008**, *178*, 4314–4325. [CrossRef]
30. Qian, X.; Hua, X.S.; Chen, P.; Ke, L. PLBP: AN effective local binary patterns texture descriptor with pyramid representation. *Pat. Rec.* **2011**, *44*, 2502–2515. [CrossRef]
31. Cortes, C.; Vapnik, V. Support-vector network. *Mach. Learn.* **1995**, *20*, 273–297. [CrossRef]
32. Wang, F.; Elbadawi, M.; Liu, S.; Tsilova, S.; Gaisford, A.W.; Basit, M. Parhizkar Machine learning to empower electrohydrodynamic processing. *Mat. Scie. Eng. C* **2022**, *132*, 112553. [CrossRef] [PubMed]
33. Kumari, P.; Basnet, B.; Wang, H.; Lavrentovich, O.D. Ferroelectric nematic liquid with coins. *Nat. Commun.* **2023**, *14*, 748. [CrossRef] [PubMed]